

## Article

# The Dynamics of Earth's Cusp in Response to the Interplanetary Shock

Jie Ren <sup>1</sup>, Qiugang Zong <sup>1,\*</sup>, Suiyan Fu <sup>1</sup>, Huigen Yang <sup>2</sup>, Zejun Hu <sup>2</sup>, Xiaoxin Zhang <sup>3</sup>, Xuzhi Zhou <sup>1</sup>, Chao Yue <sup>1</sup>, Lynn Kistler <sup>4</sup>, Patrick Daly <sup>5</sup>, Elena Kronberg <sup>6</sup> and Robert Rankin <sup>7</sup>

<sup>1</sup> Institute of Space Physics and Applied Technology, Peking University, Beijing 100871, China

<sup>2</sup> Polar Research Institute of China, Shanghai 200136, China

<sup>3</sup> Key Laboratory of Space Weather, National Center for Space Weather, China Meteorological Administration, Beijing 100081, China

<sup>4</sup> Space Science Center, University of New Hampshire, Durham, NH 03824, USA

<sup>5</sup> Max Planck Institute for Solar System Research, 37077 Göttingen, Germany

<sup>6</sup> Department of Earth and Environmental Sciences, Ludwig Maximilian University, 80333 Munich, Germany

<sup>7</sup> Department of Physics, University of Alberta, Edmonton, AB T6G 2R3, Canada

\* Correspondence: qgzong@pku.edu.cn

**Abstract:** The Earth's magnetospheric cusp, a region with an off-equatorial magnetic field minimum, is an important place which directly transports plasma and energy from the solar wind into the magnetosphere and ionosphere. Its magnetic topology and charged particles therein are known to respond to the solar wind and the interplanetary magnetic field. However, its dynamics in response to the interplanetary (IP) shock are still unknown, due to lack of direct spacecraft observations. This study first reports the observations of the cusp's motion under the drive of an IP shock and both strong electric fields and outflowing energetic ions in the moving cusp. After an IP shock arrival on 7 September 2017, triple cusps were observed by Cluster C4 when it was crossing the high-altitude northern polar region to the sub-solar magnetosphere. The multiple cusps had a one-to-one correspondence with the dayside magnetosphere compression and relaxation detected by THEMIS E, indicating that one cusp moved back and forth three times due to the IP shock's impact. In the moving cusp, there were strong impulsive electric fields with a peak of up to  $\sim 40$  mV/m and an ionospheric source population of upward propagating ions ( $O^+$ ,  $He^+$  and  $H^+$ ) with energies extending to MeV. However, the outflowing ions outside the cusp had energies of no more than 1 keV. An enhancement of energetic  $O^+$  appeared inside the cusp with the flux ratio of  $O^+/H^+$  increasing from 10 keV to  $\sim$  MeV, which implies the efficient acceleration of  $O^+$ . These observations are shown to be consistent with the prompt acceleration by the impulsive electric fields, which is mass-dependent. This finding suggests a new acceleration mechanism for cusp energetic ions, especially for  $O^+$ .

**Keywords:** triple cusps; interplanetary shock; impulsive electric field; particle acceleration; ionospheric outflows



**Citation:** Ren, J.; Zong, Q.; Fu, S.; Yang, H.; Hu, Z.; Zhang, X.; Zhou, X.; Yue, C.; Kistler, L.; Daly, P.; et al. The Dynamics of Earth's Cusp in Response to the Interplanetary Shock. *Universe* **2023**, *9*, 143. <https://doi.org/10.3390/universe9030143>

Academic Editor: Vladislav Demyanov

Received: 24 February 2023

Revised: 7 March 2023

Accepted: 7 March 2023

Published: 8 March 2023



**Copyright:** © 2023 by the authors. Licensee MDPI, Basel, Switzerland. This article is an open access article distributed under the terms and conditions of the Creative Commons Attribution (CC BY) license (<https://creativecommons.org/licenses/by/4.0/>).

## 1. Introduction

The polar cusp is an essential part of the dayside high-latitude magnetosphere which directly connects to the magnetosheath and ionosphere, and plays an important role in the coupling between the solar wind and magnetosphere [1–5]. As a boundary region located at high latitudes, the polar cusp is present whether the interplanetary magnetic field (IMF) is northward or southward [6,7]. Its location and extent are controlled by a variety of factors including the IMF direction, dipole tilt angle, solar wind azimuthal flow as well as dynamic pressure [8,9]. The cusp moves equatorward (poleward) under negative (positive) IMF  $B_z$  conditions, and the cusp location also shows a displacement dawnward (duskward) under negative (positive) IMF  $B_y$  conditions in the northern hemisphere [10]. As the solar wind pressure decreases and then increases, the cusp moves poleward and equatorward,

respectively [11,12]. According to the satellite observations, the high-altitude cusp region appears to expand and exhibit more complex behavior than the low-altitude cusp [7,13,14]. The low-altitude DMSP (Defense Meteorological Satellite Program) satellite observations revealed the existence of double cusps [15]. It was suggested to be a spatial effect where merging occurs simultaneously in the low- and high-latitude magnetopause when there is strong duskward (dawnward) IMF with small IMF  $B_z$  in the northern (southern) hemisphere. Four cusps were observed by Cluster in the high-altitude northern magnetosphere when the IMF was northward with strong duskward  $B_y$  [16]. It was explained as the main cusp was first shifted westward due to the windsock effect of the enhanced solar wind azimuthal flow and then oscillated in a similar period with the motion of a cold dense plasma sheet in the magnetotail flank due to the high-latitude reconnection. However, there are rare studies about how the cusp region responds to extreme solar wind conditions, such as an IP shock.

The diamagnetic depression (also called the diamagnetic cavity, DMC) is caused by the increases of both plasma pressure and density as a result of the magnetosheath plasma accumulation in the cusp region, which is frequently filled with energetic particles (electron, proton, multiply charged ion species, etc. [17–20]. There are three possible sources of energetic particles in the cusp DMC. The first one is called Fermi acceleration near the quasi-parallel bow shock [21–23], whereby shock-accelerated ions can be transported into the cusp region along newly reconnected field lines [17,24]. Second, simulation studies suggest that magnetospheric energetic particles may leak into the outer cusp region due to the existence of an off-equatorial magnetic field minimum [25,26]. The third mechanism is local acceleration related to gradients in reconnected quasi-potential [19] and wave–particle interactions [18,27,28]. Locally accelerated particles are distributed at pitch angles of  $\sim 90^\circ$  [19] and can exhibit higher fluxes than in the magnetosheath [19,29]. Previous studies focused on the acceleration of energetic  $H^+$ ,  $He^+$  and multiply-charged particles [17–19,30], but there have been relatively few studies of energetic  $O^+$  observations in the cusp region [31,32].

The objective of this work is to investigate the motion of the high-altitude cusp and charged particles in response to an IP shock using coordinated measurements from ACE at L1, THEMIS E in the subsolar magnetosheath as well as four Cluster satellites in the polar region of the northern hemisphere.

## 2. Observations

### 2.1. The Motion of the High-Altitude Cusp in Response to an IP Shock

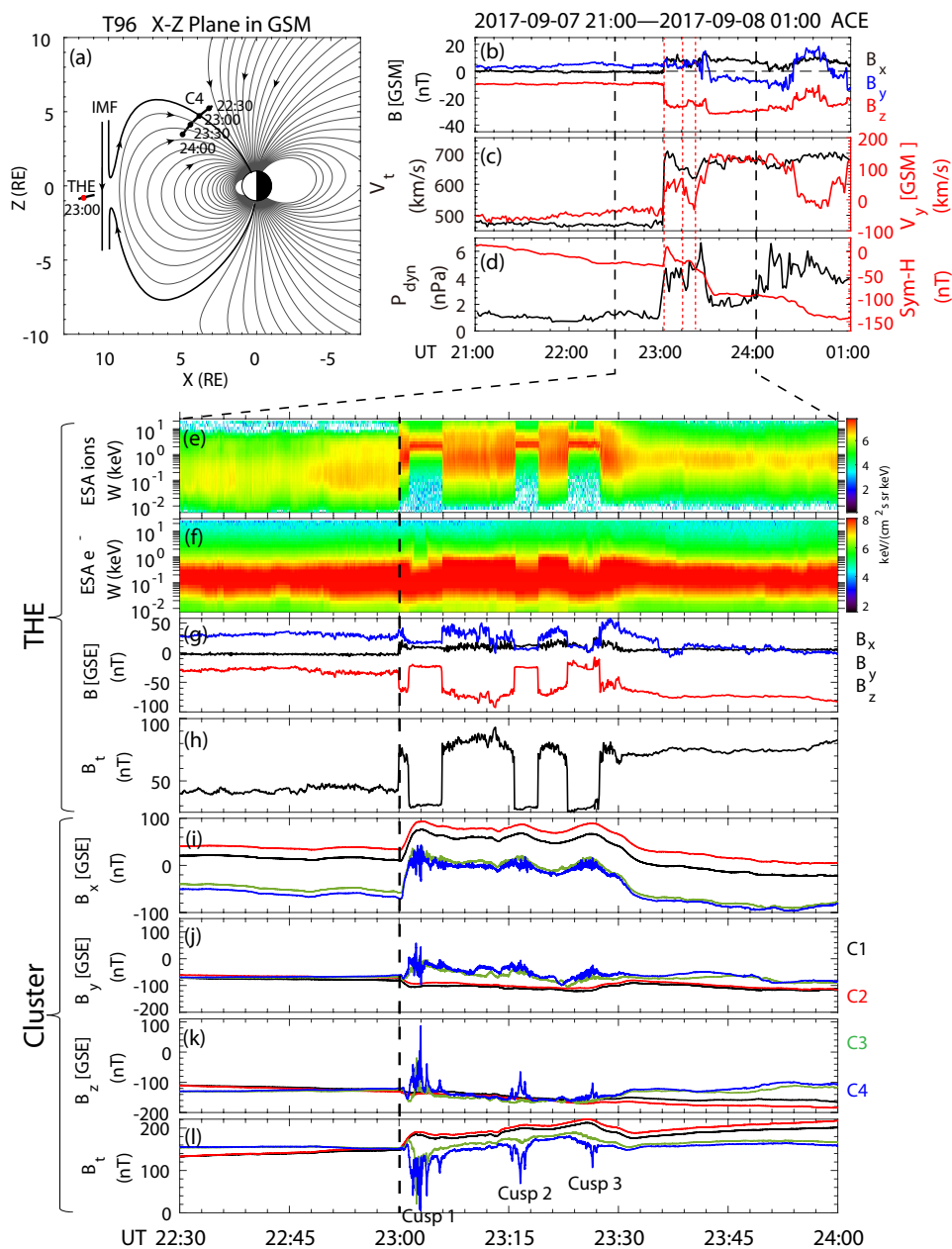
From 22:30 UT to 24:00 UT on 7 September 2017, the Cluster satellites were crossing the high-altitude northern polar region and traveling equatorward toward the subsolar region, while THEMIS E was traveling inbound in the subsolar magnetosheath. Figure 1a shows the trajectory of Cluster C4 and THEMIS E in the X-Z plane of GSM coordinates over this time span. When an IP shock arrived at Earth's magnetosphere at 23:00 UT, four Cluster satellites (C1–C4) were located at  $(1.8, 4.1, 6.1)R_E$ ,  $(0.8, 4.0, 6.5)R_E$ ,  $(3.8, 2.8, 5.1)R_E$  and  $(4.1, 2.7, 4.9)R_E$  in the GSM coordinate, respectively, while THEMIS E was located at GSM  $(11.4, 2.1, -0.7)R_E$  (marked by a red dot in Figure 1a) and ACE was located at GSM  $(224.2, 19.5, -28.4)R_E$ . C4 was followed by C3 with a separation of about  $0.3 R_E$ , followed by C1 and C2 with a time lag of  $\sim 2$  h and a separation of  $\sim 3.0 R_E$ . C3/C4 and C1/C2 were located at the magnetic local time (MLT) of about 14 h and 17 h, respectively, in the time interval from 23:00 UT to 23:30 UT, which is the time of interest in this study. The joint observations from ACE, THEMIS E and Cluster provide a good opportunity for investigating the response of the high-altitude cusp to an IP shock.

Figure 1b–d displays the ACE observations from 21:00 UT on 7 September 2017 to 01:00 UT on 8 September 2017. The time series of IMF, solar wind velocity and dynamic pressure have been time-shifted by 25 min, which was determined by the solar wind velocity and the location of ACE, as well as the sudden enhancement of Sym-H index in Figure 1d. From 23:00–23:30 UT, there was a large negative IMF  $B_z$  (about  $-25$  nT),

weak duskward IMF  $B_y$  as well as three solar wind dynamic pressure pulses together with some perturbations. Observations from THEMIS E are shown in Figure 1e–h. The spectra of ions (Figure 1e) and electrons (Figure 1f) indicate that THEMIS E was located in the magnetosheath before the shock arrival. Under the compression by the IP shock at 23:00 UT, the total magnetic field ( $B_t$ ) in the magnetosheath increased from 40 nT to 75 nT (Figure 1h) and the ion temperature was enhanced from  $\sim 0.2$  keV to  $\sim 2$  keV (Figure 1e). About 1.5 min later, the main population of ions was at several keV and  $B_t$  decreased to about 30 nT, indicating that THEMIS E was exposed to solar wind due to the further compression by the shock. The magnetic field observations from four Cluster spacecraft are shown in Figure 1i–l. When THEMIS E was exposed to solar wind just outside the magnetosheath for the first time, the cusp DMC was encountered by C3 and C4 with  $B_t$  decreased from  $>100$  nT to  $<10$  nT (referred as Cusp 1) in Figure 1l, while there was enhanced  $B_t$  at the location of C1 and C2. The decrease of  $B_t$  was observed first by C4 and then by C3, and there was a transient sign change of  $B_z$  from negative to positive. This indicates that the encounter of the cusp DMC is due to its anti-sunward motion, driven by the sudden impact of the IP shock. Although C3 and C4 were located at the MLT of about 14 h, the cusp center could move to the post-noon sector under the driving of the solar wind  $V_y$ , which jumped from  $-50$  km/s to  $+50$  km/s in Figure 1c. This is consistent with the increase of  $B_y$  observed by C3 and C4 in Figure 1j. When THEMIS E re-entered the magnetosheath at 23:06 UT, C3 and C4 successively moved outside Cusp 1, which should move sunward due to the dayside magnetosphere relaxation. Subsequently, THEMIS E went into and out of solar wind twice under the action of solar wind dynamic pressure pulses (Figure 1d); correspondingly, the cusp DMC motion back and forth was observed by C4 twice (referred as Cusp 2 and 3). Compared to Cusp 1, the diamagnetic depression in Cusp 2 and 3 is much smaller, indicating that C4 was far away from the cusp DMC center after the encounter of Cusp 1. When the solar wind dynamic pressure dramatically decreased after 23:30 UT, the magnetosheath observed by THEMIS E was no longer compressed and the moving cusp DMC did not reappear at the location of C4.

## 2.2. Energetic Ions and Impulsive Electric Fields in the Moving Cusp

The CODIF and PEACE instruments onboard Cluster provide 3D measurements of ions ( $O^+$ ,  $He^+$  and  $H^+$ ) in the energy range of  $\sim 25$  eV/e–40 keV/e [33] and electrons in the energy range of 0.6 eV–26.5 keV [34], respectively. During the events of this study, the CODIF instrument was in a mode where  $H^+$  is measured in 32 energy bins, while  $O^+$  and  $He^+$  are measured in 16 energy bins. Figure 2a–d show the  $O^+$  energy spectrum and pitch angle distributions at three representative energy channels observed by Cluster C4. The same plots for  $He^+$ ,  $H^+$  and electron are shown in Figure 2e–h, Figure 2i–l and Figure 2m–p, respectively. The energy spectra show that there was a low-energy population of  $O^+$  before 23:00 UT and after 23:30 UT, while it mainly appeared after 23:30 UT for  $He^+$  and  $H^+$ . The pitch angle distributions at 0.1 keV and other energy channels around it (not shown here) show that these low-energy ions were dominantly distributed in the antifield-aligned direction. From 23:00–23:30 UT, there were energetic  $O^+$ ,  $He^+$  and  $H^+$  in Cusp 1–3, which were mainly distributed at pitch angles of  $90^\circ$ – $180^\circ$ . These pitch angle features indicate that there were ionospheric outflows in the polar region of the northern hemisphere, which might experience perpendicular acceleration in the moving cusp DMC. It should be noted that the detailed examination of the time-of-flight spectra indicates that the intense  $H^+$  fluxes lead to contamination of the  $O^+$  measurements below 10 keV (see Figures S1 and S2 in the Supporting Information). The technique aimed at subtracting the proton “spill” from the CODIF measurements has been developed for the  $He^+$  data product [35], but there is no equivalent for  $O^+$ . The pancake-like pitch angle distribution of electrons at 0.5 keV (Figure 2o) and 1.3 keV (Figure 2n) indicates that these electrons were trapped in the cusp DMC.



**Figure 1.** (a) Trajectories of Cluster C4 and THEMIS E in the GSM XZ plane from 22:30 to 24:00 UT on 7 September 2017. The magnetospheric field lines (gray lines) are obtained by the Tsyganenko T96 model, a cartoon of the IMF field lines is marked by the black lines and the field line directions are labeled by the black arrows; (b–d) The ACE observations at L1 from 21:00 UT on 7 September 2017 to 01:00 UT on 8 September 2017, including magnetic fields, solar wind velocity and dynamic pressure/Sym-H, respectively. The vertical red lines represent the times when THEMIS E went into the solar wind, as shown in panel (e–h). The THEMIS E observations from 22:30 to 24:00 UT on 7 September 2017, including energy spectra of ion and electron, magnetic fields in GSE coordinates and total magnetic field ( $B_t$ ), respectively; (i–l) Magnetic field observations from four Cluster spacecraft. The arrival time (23:00 UT) of an IP shock is marked by the vertical dashed line.

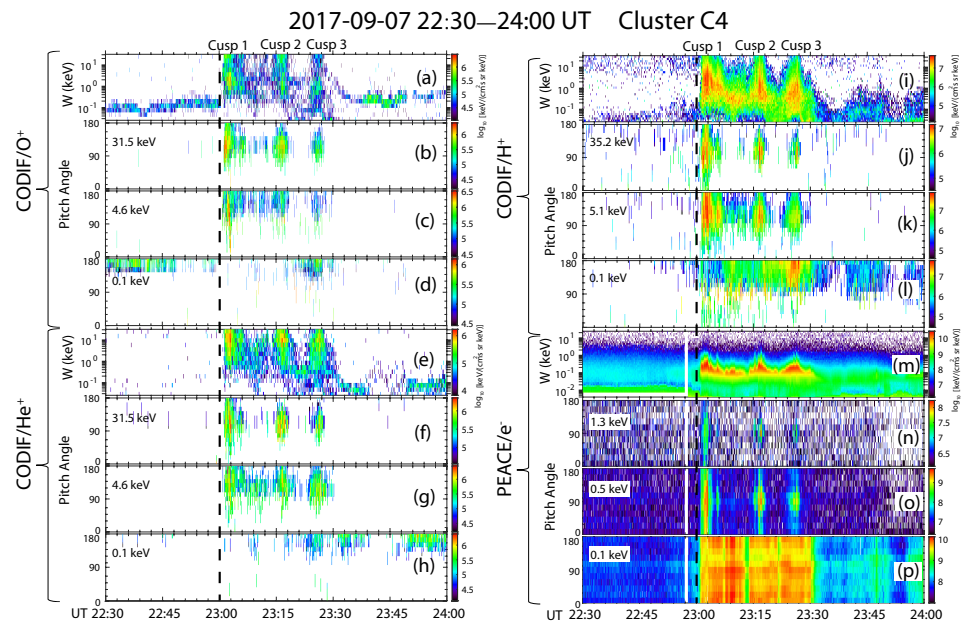


**Figure 2.** Pitch angle observations from the CODIF and PEACE instruments onboard Cluster C4 from 22:30 to 24:00 UT on 7 September 2017. (a–d) Spectrum and pitch angle distributions at three representative energy channels for  $O^+$ , respectively; The same format as panels a–d except for (e–h)  $He^+$ , (i–l)  $H^+$  and (m–p) electron. The vertical dashed line represents the shock arrival time.

Total magnetic and electric fields from Cluster C4 are shown in Figure 3a,b, respectively. There are strong electric field perturbations even up to 40 mV/m inside Cusp 1, which are comparable to those related to the shock impact around 23:01 UT. The RAPID instrument onboard Cluster C4 provides measurements of different ions from tens of keV to several MeV [36,37]. Figure 3c–h display the energy flux ( $keV/(cm^2 \cdot s \cdot sr \cdot keV)$ ) of different ions in the energy range from tens of eV to several MeV with some gaps in the energy coverage, observed by the RAPID and CODIF instruments. The RAPID measurements in Figure 3c,e,g show that energetic  $O^+$ ,  $He^+$  and  $H^+$  were mainly distributed around the region with largest magnetic depression inside Cusp 1–3. The upper energy limit of  $O^+$  extends to the MeV range in Cusp 1, which is larger than  $He^+$  and  $H^+$ . Figure 3b shows that  $E_t$  was enhanced up to  $\sim 30$  mV/m after the IP shock arrival at 23:00 UT, and showed another peak up to  $\sim 40$  mV/m around the dip of Cusp 1, which is sufficient to cause ion acceleration.

The energy increase caused by electric fields can be estimated using [38,39]

$$W = \frac{1}{2} m_i \left( \frac{\mathbf{E} \times \mathbf{B}}{B^2} + \frac{m_i}{q B^2} \frac{d\mathbf{E}_\perp}{dt} \right)^2 \quad (1)$$

where  $E$  is electric field,  $B$  is magnetic field,  $m_i$  is ion mass and  $q$  is particle charge. Here two terms on the right hand side of Equation (1) are referred as  $W_1$  ( $\mathbf{E} \times \mathbf{B}$  drift) and  $W_2$  (polarization drift), respectively. In order to compare with ion measurements, the calculated  $W$  in Equation (1) is averaged at the time resolution of CODIF and RAPID instruments. The pink line in Figure 3c,d represents the calculated  $W$  for  $O^+$ . Its maximum value is about 0.91 MeV, where  $W_1 = 22.3$  keV and  $W_2 = 889.4$  keV. So  $O^+$  can be accelerated to high energies by electric fields, which is mainly attributed to the polarization drift around the largest magnetic depression of the moving cusp DMC. The calculated  $W$  for  $He^+$  and  $H^+$  are marked by the pink lines in Figure 3e,h, respectively. Its value for  $O^+$ ,  $He^+$  and  $H^+$  in the same cusp is rapidly decreasing as ion mass is smaller, which is mainly due to the mass-dependent polarization drift. The source and acceleration mechanism of energetic ions in the moving cusp will be further discussed in the next section.

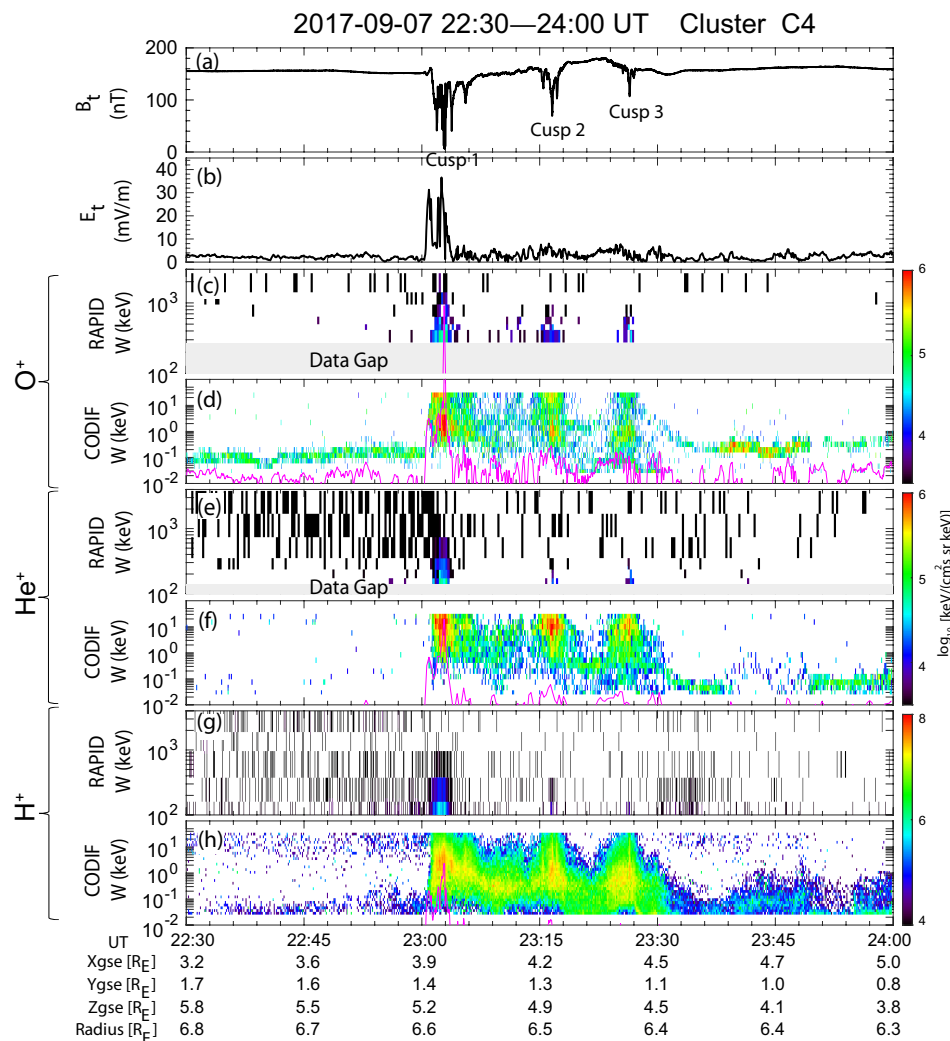


**Figure 3.** (a) Total magnetic field; (b) Total electric field; (c,d) O<sup>+</sup> spectra from the RAPID and CODIF instruments, respectively; The same format as panels b–c except for (e,f) He<sup>+</sup> and (g,h) H<sup>+</sup>. The pink line over-plotted on the ion spectrum is the energy increase caused by electric field, estimated with Equation (1). The vertical dashed line represents the shock arrival time.

### 3. Discussion

Previous statistical studies found that the cusp location at different altitudes moves equatorward with increasing southward IMF and solar wind dynamic pressure, which are interpreted in terms of the erosion of dayside magnetic flux [7,10,40] and the global expansion of the cusp region [11,12], respectively. The response of the cusp region to extreme solar wind conditions such as an IP shock is rarely studied. The observations in Figure 1 showed that after the IP shock arrival with large IMF B<sub>z</sub> and solar wind dynamic pressure, the dayside magnetosphere was severely compressed and the whole cusp region moved anti-sunward. The influence of the sudden solar wind dynamic pressure on the cusp location exceeds the erosion and expansion processes under the steady solar wind conditions. Previous studies suggested that multiple cusps can be attributed to a spatial effect [15], a temporal effect [14,16], or a combination of the two [14]. The spatial effect cannot account for the triple cusps in this study, because it works when there is strong dawnward/duskward and weak southward IMF [15]. Zong et al. [14,16] suggested that the solar wind azimuthal flow was a stronger controlling factor of the cusp position than the IMF B<sub>y</sub> and B<sub>z</sub>, which plays a crucial role in the appearance of multiple cusps in this study. The jump of the solar wind V<sub>y</sub> from −50 km/s to 50 km/s in Figure 1c can shift the cusp region to the post-noon sector where four Cluster satellites were located, but it should not

be the determinant of the observed triple cusps. The triple cusps occurred when the solar wind dynamic pressure was high from 23:00 UT to 23:30 UT, and each cusp corresponded to one dayside magnetosphere compression and relaxation. The cusp was not encountered again by Cluster spacecraft after 23:30 UT when the solar wind  $V_y$  became even larger, and the solar wind dynamic pressure decreased. The joint observations from ACE, THEMIS and Cluster in Figure 1 revealed that the appearance of triple cusps in this study is attributed to the successive compression and relaxation effect caused by the dynamic pressure of the IP shock.

Inside the cusp, energetic ions ( $O^+$ ,  $He^+$  and  $H^+$ ) with energy up to MeV were observed by Cluster C4. The measurement of energetic  $O^+$  is a good indicator for an ionospheric source [17,41,42]. The pitch angles of these energetic ions in Figure 2 indicate that they should originate from ionosphere [32]. The energies of ions outside the cusp were no more than 1 keV and mainly distributed in the antifield-aligned direction. However, the pitch angles of energetic ions inside the cusp are closer to  $90^\circ$ , which suggests acceleration in the perpendicular direction. The calculations with Equation (1) in Figure 3 imply that the impulsive acceleration by electric fields can account for the energy increase of ions inside the cusp. Although there was long stable southward IMF and continuous decrease of the SML index before the IP shock arrival, there were no substorm injections and enhancement of energetic particles in the magnetosphere (see Figure S3 in the supporting information). Moreover, there are almost no energetic ions at the pitch angles of  $90^\circ$ – $180^\circ$  inside the cusp of the northern hemisphere. Schillings et al. [32] suggested that these ions in the same event were ionospheric outflows due to a preheating of the ionosphere by the multiple X-flares. Therefore, it is unlikely that the cusp energetic ions in Figure 3 should originate from the nightside substorm injections that can drift to the dayside magnetopause and access the field lines, which ultimately become cusp field lines.

The energy flux spectra of different ions can help verify whether there is impulsive electric field acceleration or not. Figure 4a–c shows the energy flux spectra of  $O^+$ ,  $He^+$  and  $H^+$ , respectively, around the minimum  $B_t$  in Cusp 1. The largest magnetic depression occurred at about 23:02:54 UT. In Figure 4a–c, the energy fluxes averaged within half a minute from 23:02:40 UT to 23:03:10 UT are marked by pink dots with error bars. There are two populations (Part I and II) separated by 10 keV for  $O^+$ , while there is only one population for both  $He^+$  and  $H^+$ . A detailed examination of the time-of-flight spectrum indicates that the first  $O^+$  peak is actually contamination due to the intense  $H^+$  flux. However, the higher energy peak represents true  $O^+$ . The spectra of  $O^+$ ,  $He^+$  and  $H^+$  can be fitted to a kappa distribution to obtain more information, which is given by [39,43]

$$f(W) = n \left( \frac{m}{2\pi\kappa W_0} \right)^{3/2} \frac{\Gamma(\kappa + 1)}{\Gamma(\kappa - 1/2)} \left( 1 + \frac{(\sqrt{W} - \sqrt{W_s})^2}{\kappa W_0} \right)^{-(\kappa+1)} \quad (2)$$

where  $f$ ,  $n$ ,  $m$ ,  $W$  are particle phase space density, density, mass, and energy, respectively;  $W_s$  is the so-called shift energy;  $W_0$  is the most probable energy related to the average thermal energy by  $W_0 = k_B T (1 - \frac{3}{2\kappa})$ . For  $\kappa \rightarrow \infty$ , the kappa distribution degenerates to a simple Maxwellian; for  $\kappa > 1$ , a smaller  $\kappa$  indicates a harder tail. The black lines in Figure 4a–c represent the fitting spectra, and the fitting parameters are marked in the legend of these figures. Figure 4d shows the flux ratios of  $O^+/H^+$  and  $He^+/H^+$  obtained from the observations and fitting results in Figure 4a–c. The flux ratios of  $O^+/H^+$  shows an increasing trend from 10 keV to  $\sim$  MeV, which demonstrates the efficient acceleration of  $O^+$ .

The fitting results show that the  $\kappa$  index values for  $O^+$ ,  $He^+$  and  $H^+$  are much less than 10, indicating that they have an enhanced tail due to acceleration [43]. The smaller  $\kappa$  for the high-energy population (Part II) of  $O^+$  implies that these energetic  $O^+$  undergo a further acceleration. The maximum values of the calculated  $W$  in Figure 3 are marked with red texts and arrows in Figure 4a–c. The energy increase caused by electric fields in the moving cusp DMC is enough to account for the formation of a high-energy population of  $O^+$ . It should be noted that the impulsive acceleration by electric fields in the cusp is much

more complex than that shown in Equation (1), as indicated by the comparisons between ion observations and theoretical calculations in Figures 3 and 4, which are probably due to (1) the finite gyro-radius effect, (2) the potential re-acceleration, and (3) the spatial spread of ion distribution associated with their motions (gyration, bounce and drift) in the cusp. In addition, electric fields at different positions of a moving cusp should be changing in real time so that the electric field acceleration of energetic ions can only be estimated roughly with single-point measurements.

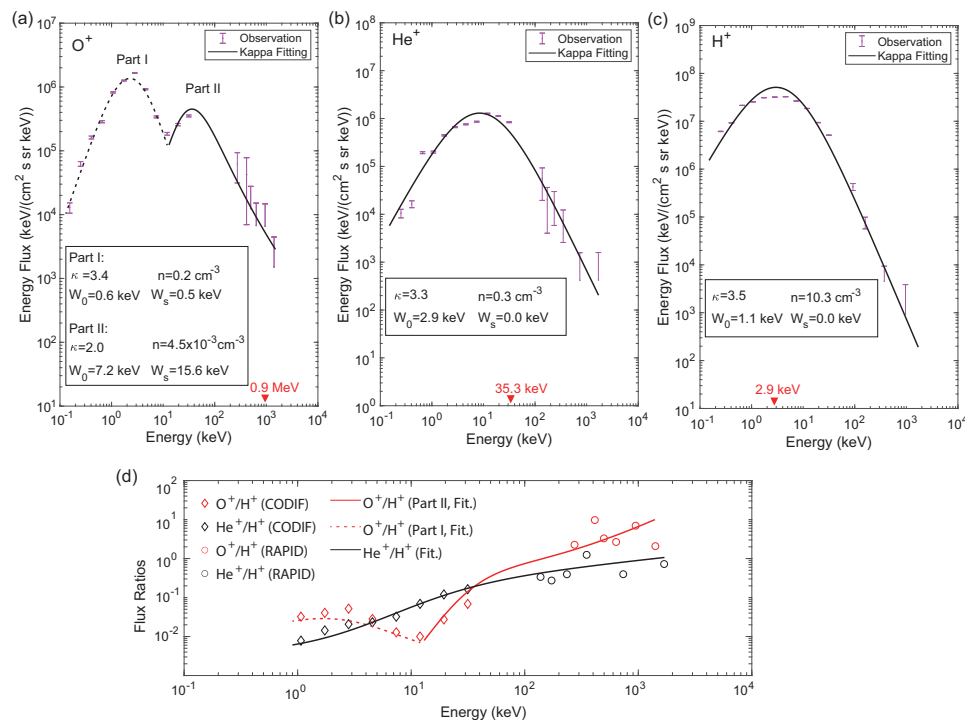


**Figure 4.** (a–c) The energy flux spectra of O<sup>+</sup>, He<sup>+</sup> and H<sup>+</sup> around the minimum B<sub>t</sub> in Cusp 1, respectively. The largest magnetic depression occurred at about 23:02:54 UT. The pink dots with error bars are the averaged energy fluxes between 23:02:40 UT and 23:03:10 UT. The black lines represent the best fit of the energy fluxes with the kappa distribution, and the fitting parameters are marked in the legend. The red arrows represent the maximum energy increase in Cusp 1 caused by electric fields in Figure 3. (d) The flux ratios of O<sup>+</sup>/H<sup>+</sup> and He<sup>+</sup>/H<sup>+</sup>. The marks and lines represent the measurements and fitting results in panels (a–c), respectively. Since the central energies of each channel for O<sup>+</sup>, He<sup>+</sup> and H<sup>+</sup> from the CODIF and RAPID instrument are different, H<sup>+</sup> fluxes are first interpolated and then used to calculate the flux ratios. It should be noted that we adopt the background values of H<sup>+</sup> in the energy channels of 962 keV and 1885 keV, and He<sup>+</sup> in the energy channels of 737 keV and 1689 keV, which are the averages from 23:00 to 23:05 UT, because most of the measurements from 23:02:40–23:03:10 UT are absent. Considering that the first O<sup>+</sup> peak (Part I) is actually contamination due to the intense H<sup>+</sup>, the fitting result is marked by a dashed line in panels (a,d).

It is well known that when the IP shock impinges on the magnetosphere [44] and substorm activities occur [45], impulsive electric fields can be induced by the local magnetic field reconfiguration, and numerous studies demonstrated their crucial role in the prompt acceleration and enhanced transportation of both radiation belt electrons and ring current ions [46,47]. This study reveals the existence of large (~40 mV/m peak) impulsive electric fields in the cusp region under the impact of an IP shock, which are comparable to those observed in the inner magnetosphere [46] and in the near-Earth plasma sheet [45]. It is reasonable to believe that such strong electric fields induced by the rapid change of magnetic fields in the magnetospheric cusp, which is a very large and dynamic region extending in three dimensions [48–50], can produce significant energization of charged particles. This

study suggests a new acceleration mechanism for cusp energetic particles according to spacecraft observations, but the detailed acceleration process and the actual impact need further investigation with the aid of simulations. Conceivably, since the magnetic field lines in the cusp are connected to all of the magnetopause boundary layers, these energetic particles probably make important global impacts on the geospace environment.

#### 4. Conclusions

In the time interval from 23:00 UT to 23:30 UT on 7 September 2017, the joint observations from ACE at L1, THEMIS E in the subsolar magnetosheath, and Cluster spacecraft in the high-altitude polar region of the northern hemisphere shed new light on understanding the dynamics of the cusp in response to an IP shock. The main results are summarized as follows:

1. According to the ACE observations, an IP shock arrived at Earth's magnetosphere at about 23:00 UT, together with strong solar wind dynamic pressure pulses and large southward IMF. Under the impact of the IP shock, THEMIS E in the subsolar magnetosheath went into solar wind three times from 23:00–23:30 UT, indicating that there were successive dayside magnetosphere compressions and relaxations. Meanwhile, triple cusps were observed by Cluster C4, and each encounter had a good one-to-one correspondence with the dayside magnetosphere compression and relaxation. Therefore, this multiple cusp phenomenon can be attributed to a temporal effect that the same cusp is moving back and forth three times under the driving of the solar wind dynamic pressure.
2. In the moving cusp, there were strong electric field perturbations up to 40 mV/m and energetic ions ( $O^+$ ,  $He^+$  and  $H^+$ ) up to MeV. These energetic ions were mainly distributed at pitch angles of  $90^\circ$ – $180^\circ$ , while there were low-energy ions (no more than 1 keV) in the antipolar-aligned direction outside the cusp. These pitch angle features of different ions and the observations of the  $O^+$  population imply that energetic ions in the moving cusp originate from the ionospheric outflows, which should experience further perpendicular acceleration in the upward process.
3. Strong electric field perturbations and weak total magnetic field in the moving cusp can cause much more remarkable energy increase of  $O^+$  than light ions ( $He^+$  and  $H^+$ ), mainly due to the polarization drift. In other words, the impulsive acceleration by electric fields is mass-dependent, which can lead to the fast formation of a high-energy population of  $O^+$ . The ratio of  $O^+/H^+$  is increasing from 10 keV to MeV, indicating the efficient acceleration of  $O^+$ . The agreement between the observations and estimates based on Equation (1) supports the conclusion that impulsive acceleration by electric fields in the moving cusp could play a crucial role in the dynamics of energetic ions, especially for  $O^+$ .

**Supplementary Materials:** The following supporting information can be downloaded at: <https://www.mdpi.com/article/10.3390/universe9030143/s1>, Figure S1: The CODIF time-of-flight (TOF) spectra for all energies as function of TOF channel and energy during different time intervals; Figure S2: The TOF spectra as function of TOF channel and normalized pulse-height counts in different energy step ranges during 23:00–23:30 UT; Figure S3: The observations of energetic electrons from GOES13 and energetic  $O^+$  from Van Allen Probe A.

**Author Contributions:** Conceptualization, J.R., Q.Z. and S.F.; methodology, J.R., X.Z. (Xuzhi Zhou) and C.Y.; software, J.R.; validation, H.Y., Z.H. and X.Z. (Xiaoxin Zhang); formal analysis, J.R. and Q.Z.; investigation, J.R. and R.R.; resources, Q.Z.; data curation, L.K., P.D. and E.K.; writing—original draft preparation, J.R.; writing—review and editing, Q.Z., S.F., H.Y. and X.Z. (Xuzhi Zhou); visualization, J.R.; supervision, Q.Z. and L.K.; project administration, J.R. and Q.Z.; funding acquisition, J.R. and Q.Z. All authors have read and agreed to the published version of the manuscript.

**Funding:** This work was supported by the National Natural Science Foundation of China (grant numbers 42230202, 42274202, 41731068, 41974191 and 41931073) and the National Key R&D Program of China (grant number 2021YFA0718600).

**Data Availability Statement:** The Cluster data are available at the Cluster Science Archive website (<https://csa.esac.esa.int/csa-web/>, accessed on 10 July 2022). The ACE and THEMIS data are obtained from the Coordinated Data Analysis Web (<https://cdaweb.gsfc.nasa.gov/>, accessed on 10 July 2022).

**Conflicts of Interest:** The authors declare no conflict of interest.

## References

- Frank, L.A. Plasma in the earth's polar magnetosphere. *J. Geophys. Res.* **1971**, *76*, 5202–5219. [[CrossRef](#)]
- Newell, P.T.; Meng, C.I. The cusp and the cleft/boundary layer: Low-altitude identification and statistical local time variation. *J. Geophys. Res.* **1988**, *93*, 14549–14556. [[CrossRef](#)]
- Maynard, N.C. Coupling the solar-wind/IMF to the ionosphere through the high latitude cusps. *Surv. Geophys.* **2005**, *26*, 255–280. [[CrossRef](#)]
- Zong, Q.; Fritz, T.; Korth, A.; Daly, P.; Dunlop, M.; Balogh, A.; Fennell, J.; Sullivan, J.; Friedel, R.; Reme, H. Energetic electrons as a field line topology tracer in the high latitude boundary/cusp region: Cluster rapid observations. *Surv. Geophys.* **2005**, *26*, 215–240. [[CrossRef](#)]
- Dunlop, M.; Lavraud, B.; Cargill, P.; Taylor, M.; Balogh, A.; Réme, H.; Decreau, P.; Glassmeier, K.H.; Elphic, R.; Bosqued, J.M.; et al. Cluster observations of the cusp: Magnetic structure and dynamics. *Surv. Geophys.* **2005**, *26*, 5–55. [[CrossRef](#)]
- Russell, C. The polar cusp. *Adv. Space Res.* **2000**, *25*, 1413–1424. [[CrossRef](#)]
- Zhou, X.; Russell, C.; Le, G.; Fuselier, S.; Scudder, J. Solar wind control of the polar cusp at high altitude. *J. Geophys. Res.* **2000**, *105*, 245–251. [[CrossRef](#)]
- Tsyganenko, N.; Russell, C. Magnetic signatures of the distant polar cusps: Observations by Polar and quantitative modeling. *J. Geophys. Res.* **1999**, *104*, 24939–24955. [[CrossRef](#)]
- Měrka, J.; Šafránková, J.; Němeček, Z. Cusp-like plasma in high altitudes: A statistical study of the width and location of the cusp from Magion-4. *Ann. Geophys.* **2002**, *20*, 311–320. [[CrossRef](#)]
- Newell, P.T.; Meng, C.I.; Sibeck, D.G.; Lepping, R. Some low-altitude cusp dependencies on the interplanetary magnetic field. *J. Geophys. Res.* **1989**, *94*, 8921–8927. [[CrossRef](#)]
- Newell, P.T.; Meng, C.I. Ionospheric projections of magnetospheric regions under low and high solar wind pressure conditions. *J. Geophys. Res.* **1994**, *99*, 273–286. [[CrossRef](#)]
- Yamauchi, M.; Nilsson, H.; Eliasson, L.; Norberg, O.; Boehm, M.; Clemmons, J.; Lepping, R.; Blomberg, L.; Ohtani, S.I.; Yamamoto, T.; et al. Dynamic response of the cusp morphology to the solar wind: A case study during passage of the solar wind plasma cloud on February 21, 1994. *J. Geophys. Res.* **1996**, *101*, 24675–24687. [[CrossRef](#)]
- Kremser, G.; Lundin, R. Average spatial distributions of energetic particles in the midaltitude cusp/cleft region observed by Viking. *J. Geophys. Res.* **1990**, *95*, 5753–5766. [[CrossRef](#)]
- Zong, Q.G.; Fritz, T.; Zhang, H.; Korth, A.; Daly, P.; Dunlop, M.; Glassmeier, K.H.; Reme, H.; Balogh, A. Triple cusps observed by Cluster—Temporal or spatial effect? *Geophys. Res. Lett.* **2004**, *31*, L09810. [[CrossRef](#)]
- Wing, S.; Newell, P.T.; Ruohoniemi, J.M. Double cusp: Model prediction and observational verification. *J. Geophys. Res.* **2001**, *106*, 25571–25593. [[CrossRef](#)]
- Zong, Q.G.; Zhang, H.; Fritz, T.; Goldstein, M.; Wing, S.; Keith, W.; Winningham, J.; Frahm, R.; Dunlop, M.; Korth, A.; et al. Multiple cusps during an extended northward IMF period with a significant By component. *J. Geophys. Res.* **2008**, *113*. [[CrossRef](#)]
- Trattner, K.; Fuselier, S.; Peterson, W.; Chang, S.W.; Friedel, R.; Aellig, M. Origins of energetic ions in the cusp. *J. Geophys. Res.* **2001**, *106*, 5967–5976. [[CrossRef](#)]
- Chen, J.; Fritz, T.A. Correlation of cusp MeV helium with turbulent ULF power spectra and its implications. *Geophys. Res. Lett.* **1998**, *25*, 4113–4116. [[CrossRef](#)]
- Nykyri, K.; Otto, A.; Adamson, E.; Kronberg, E.; Daly, P. On the origin of high-energy particles in the cusp diamagnetic cavity **2012**, *87*, 70–81. [[CrossRef](#)]
- Burkholder, B.; Nykyri, K.; Ma, X. Magnetospheric multiscale statistics of high energy electrons trapped in diamagnetic cavities. *J. Geophys. Res.* **2021**, *126*, e2020JA028341. [[CrossRef](#)]
- Gosling, J.; Thomsen, M.; Bame, S.; Russell, C. On the source of diffuse, suprathermal ions observed in the vicinity of the Earth's bow shock. *J. Geophys. Res.* **1989**, *94*, 3555–3563. [[CrossRef](#)]
- Lee, M.A. Coupled hydromagnetic wave excitation and ion acceleration upstream of the Earth's bow shock. *J. Geophys. Res.* **1982**, *87*, 5063–5080. [[CrossRef](#)]
- Ellison, D.C.; Moebius, E.; Paschmann, G. Particle injection and acceleration at earth's bow shock—Comparison of upstream and downstream events. *Astrophys. J.* **1990**, *352*, 376–394. [[CrossRef](#)]
- Chang, S.W.; Scudder, J.; Fuselier, S.; Fennell, J.; Trattner, K.; Pickett, J.; Spence, H.E.; Menietti, J.; Peterson, W.; Lepping, R.; et al. Cusp energetic ions: A bow shock source. *Geophys. Res. Lett.* **1998**, *25*, 3729–3732. [[CrossRef](#)]
- Delcourt, D.; Sauvaud, J.A. Populating of the cusp and boundary layers by energetic (hundreds of keV) equatorial particles. *J. Geophys. Res.* **1999**, *104*, 22635–22648. [[CrossRef](#)]

26. Zhou, X.Z.; Fritz, T.; Zong, Q.G.; Pu, Z.; Hao, Y.Q.; Cao, J.B. The cusp: A window for particle exchange between the radiation belt and the solar wind. *Ann. Geophys.* **2006**, *24*, 3131–3137. [[CrossRef](#)]
27. Nykyri, K.; Cargill, P.; Lucek, E.; Horbury, T.; Lavraud, B.; Balogh, A.; Dunlop, M.; Bogdanova, Y.; Fazakerley, A.; Dandouras, I.; et al. Cluster observations of magnetic field fluctuations in the high-altitude cusp. *Ann. Geophys.* **2004**, *22*, 2413–2429. [[CrossRef](#)]
28. Grison, B.; Sahraoui, F.; Lavraud, B.; Chust, T.; Cornilleau-Wehrlin, N.; Reme, H.; Balogh, A.; André, M. Wave particle interactions in the high-altitude polar cusp: A Cluster case study. *Ann. Geophys.* **2005**, *23*, 3699–3713. [[CrossRef](#)]
29. Chen, J.; Fritz, T.A. High-altitude cusp: The extremely dynamic region in geospace. *Surv. Geophys.* **2005**, *26*, 71–93. [[CrossRef](#)]
30. Zhang, H.; Fritz, T.; Zong, Q.G.; Daly, P. Stagnant exterior cusp region as viewed by energetic electrons and ions: A statistical study using Cluster Research with Adaptive Particle Imaging Detectors (RAPID) data. *J. Geophys. Res.* **2005**, *110*, A05211. [[CrossRef](#)]
31. Nykyri, K.; Otto, A.; Adamson, E.; Dougal, E.; Mumme, J. Cluster observations of a cusp diamagnetic cavity: Structure, size, and dynamics. *J. Geophys. Res.* **2011**, *116*, A03228. [[CrossRef](#)]
32. Schillings, A.; Nilsson, H.; Slapak, R.; Wintoft, P.; Yamauchi, M.; Wik, M.; Dandouras, I.; Carr, C.M. O<sup>+</sup> escape during the extreme space weather event of 4–10 September 2017. *Space Weather* **2018**, *16*, 1363–1376. [[CrossRef](#)]
33. Rème, H.; Aoustin, C.; Bosqued, J.M.; Dandouras, I.; Lavraud, B.; Sauvaud, J.A.; Barthe, A.; Bouyssou, J.; Camus, T.; Coeur-Joly, O.; et al. First multispacecraft ion measurements in and near the Earth's magnetosphere with the identical Cluster ion spectrometry (CIS) experiment. *Ann. Geophys.* **2001**, *19*, 1303–1354. [[CrossRef](#)]
34. Johnstone, A.; Alsop, C.; Burge, S.; Carter, P.; Coates, A.; Coker, A.; Fazakerley, A.; Grande, M.; Gowen, R.; Gurgiolo, C.; et al. *PEACE: A Plasma Electron and Current Experiment*; Springer: Berlin/Heidelberg, Germany, 1997; pp. 351–398.
35. Mouikis, C.; Kistler, L.; Wang, G.; Liu, Y. Background subtraction for the Cluster/CODIF plasma ion mass spectrometer. *Geosci. Instrum. Methods Data Syst.* **2014**, *3*, 41–48. [[CrossRef](#)]
36. Wilken, B.; Daly, P.; Mall, U.; Aarsnes, K.; Baker, D.; Belian, R.; Blake, J.; Borg, H.; Büchner, J.; Carter, M.; et al. First results from the RAPID imaging energetic particle spectrometer on board Cluster. *Ann. Geophys.* **2001**, *19*, 1355–1366. [[CrossRef](#)]
37. Zong, Q.G.; Wang, Y.F.; Zhang, H.; Fu, S.Y.; Zhang, H.; Wang, C.R.; Yuan, C.J.; Vogiatzis, I. Fast acceleration of inner magnetospheric hydrogen and oxygen ions by shock induced ULF waves. *J. Geophys. Res.* **2012**, *117*, A11206. [[CrossRef](#)]
38. Liu, Z.Y.; Zong, Q.G.; Zhou, X.Z.; Hao, Y.; Yau, A.; Zhang, H.; Chen, X.R.; Fu, S.; Pollock, C.; Le, G.; et al. ULF waves modulating and acting as mass spectrometer for dayside ionospheric outflow ions. *Geophys. Res. Lett.* **2019**, *46*, 8633–8642. [[CrossRef](#)]
39. Baumjohann, W.; Treumann, R.A. *Basic Space Plasma Physics*; World Scientific: Singapore, 1997.
40. Palmroth, M.; Laakso, H.; Pulkkinen, T. Location of high-altitude cusp during steady solar wind conditions. *J. Geophys. Res.* **2001**, *106*, 21109–21122. [[CrossRef](#)]
41. Yau, A.; André, M. Sources of ion outflow in the high latitude ionosphere. *Space Sci. Rev.* **1997**, *80*, 1–25. [[CrossRef](#)]
42. Zurbuchen, T.; Fisk, L.; Gloeckler, G.; Von Steiger, R. The solar wind composition throughout the solar cycle: A continuum of dynamic states. *Geophys. Res. Lett.* **2002**, *29*, 661–664. [[CrossRef](#)]
43. Pierrard, V.; Lazar, M. Kappa distributions: Theory and applications in space plasmas. *Sol. Phys.* **2010**, *267*, 153–174. [[CrossRef](#)]
44. Zhang, D.; Liu, W.; Li, X.; Sarris, T.; Xiao, C.; Wygant, J.R. Observations of impulsive electric fields induced by interplanetary shock. *Geophys. Res. Lett.* **2018**, *45*, 7287–7296. [[CrossRef](#)]
45. Aggson, T.; Heppner, J.; Maynard, N. Observations of large magnetospheric electric fields during the onset phase of a substorm. *J. Geophys. Res.* **1983**, *88*, 3981–3990. [[CrossRef](#)]
46. Li, X.; Roth, I.; Temerin, M.; Wygant, J.; Hudson, M.; Blake, J. Simulation of the prompt energization and transport of radiation belt particles during the March 24, 1991 SSC. *Geophys. Res. Lett.* **1993**, *20*, 2423–2426. [[CrossRef](#)]
47. Nosé, M.; Keika, K.; Kletzing, C.; Spence, H.; Smith, C.; MacDowall, R.; Reeves, G.D.; Larsen, B.; Mitchell, D. Van Allen Probes observations of magnetic field dipolarization and its associated O<sup>+</sup> flux variations in the inner magnetosphere at L < 6.6. *J. Geophys. Res.* **2016**, *121*, 7572–7589. [[CrossRef](#)]
48. Lavraud, B.; Fedorov, A.; Budnik, E.; Thomsen, M.; Grigoriev, A.; Cargill, P.; Dunlop, M.; Reme, H.; Dandouras, I.; Balogh, A. High-altitude cusp flow dependence on IMF orientation: A 3-year Cluster statistical study. *J. Geophys. Res.* **2005**, *110*, A02209. [[CrossRef](#)]
49. Lavraud, B.; Reme, H.; Dunlop, M.; Bosqued, J.M.; Dandouras, I.; Sauvaud, J.A.; Keiling, A.; Phan, T.; Lundin, R.; Cargill, P.; et al. Cluster observes the high-altitude cusp region. *Surv. Geophys.* **2005**, *26*, 135–175. [[CrossRef](#)]
50. Zhang, B.; Brambles, O.; Lotko, W.; Dunlap-Shohl, W.; Smith, R.; Wiltberger, M.; Lyon, J. Predicting the location of polar cusp in the Lyon-Fedder-Mobarry global magnetosphere simulation. *J. Geophys. Res.* **2013**, *118*, 6327–6337. [[CrossRef](#)]

**Disclaimer/Publisher's Note:** The statements, opinions and data contained in all publications are solely those of the individual author(s) and contributor(s) and not of MDPI and/or the editor(s). MDPI and/or the editor(s) disclaim responsibility for any injury to people or property resulting from any ideas, methods, instructions or products referred to in the content.